

Colloid Formation Resulting from Highly Alkaline and Saline Waste Tank Solution Leaking into Sediments at the Hanford Site

Jiamin Wan^{1*}, Tetsu K. Tokunaga¹, Eduardo Saiz², Keith R. Olson¹, and Joern T. Larsen¹,

1. Earth Science Division, Lawrence Berkeley National Laboratory, Berkeley, CA 94720
2. Material Science Division, Lawrence Berkeley National Laboratory, Berkeley, CA 94720

ABSTRACT

Leakage of a highly alkaline and saline waste-tank solution into underlying Hanford sediments was simulated in laboratory columns at elevated (70°C) and ambient (21°C) temperatures, and followed by a simulated rainfall leaching. Three major reaction stages were identified for the sediment permeated with the waste-solution: the reaction front stage (RFS of the waste plume), the early waste-plume stage (EPS), and the late waste-plume stage (LPS); each having distinct chemical and mineralogical signatures. At the RFS, maximum geochemical disequilibrium promoted rapid silicate dissolution, cation exchange of Na replacing Ca, and precipitation. The rapid silicate dissolution resulted in a substantial pH reduction of waste solution (from 14 to ~ 8). Rapid precipitation of Si, Al, and Ca resulted in a predominantly amorphous and fine sized (20 to 500 nm) particles and their aggregates. Maximum transport of secondary colloids occurred at the RFS, documented by the large turbidity peak and highest particle counts. At the EPS, silicate dissolution continued at decreased rates, reflected by a quick return to high pH. Nitrate-cancrinite and zeolite were the dominant secondary phases throughout the entire plume stage (EPS and LPS). Because of the coatings deposited during the traverse of the RFS and the EPS, silicate dissolution rates during the LPS declined to such low levels that

changes in solution pH were no longer measurable. Leaching with dilute soil water did not remobilize measurable secondary colloids.

I. INTRODUCTION

Leakage of underground tanks containing high-level radioactive wastes has been identified at various U.S. Department of Energy facilities (1). At the Hanford Site in Washington State, about $2 \times 10^5 \text{ m}^3$ of high-level radioactive and hazardous wastes are stored in 177 underground tanks, including 149 single-shell tanks (SXT). Over time, about 67 of the SXTs developed leaks. About 2,300 to 3,400 m^3 of tank waste solution (TWS) have leaked (2). Radionuclides and other contaminants have been found at elevated concentrations in the vadose zone and groundwater beneath the SXT farm, with REDOX waste solution as the carrier (3). The nature of pathways and mechanisms responsible for deep-vadose-zone contaminant transport are not yet fully understood, and such understanding is urgently needed for future remediation.

Besides carrying fission products, the REDOX waste solution was highly alkaline and caustic, containing high concentrations of sodium, aluminum, and nitrate (4-6). Heat released from radioactive decay caused tank waste solutions to boil, and temperatures were sustained above ambient levels for a long period of time. Because of their extreme chemical-physical conditions, release of REDOX tank solutions into the underlying sediments resulted in dissolution of the primary silicate minerals and precipitation of secondary minerals. Serne et al. (7) observed formation of precipitates in effluent samples collected from flow through column tests. Nyman et al. (8) observed formation of cancrinite upon reaction of tank solutions with

Hanford sediments. Bickmore et al. (9) reported the equilibrium constant for cancrinite precipitation during reactions of quartz sand and simulated Hanford tank solutions. Depending on their physical and chemical properties, the secondary phases can associate with contaminants from the tank liquids through co-precipitation and adsorption. Subsequent colloid transport may have contributed to the deep migration of contaminants. It is believed that transport of certain low-solubility and highly sorptive contaminants in subsurface environments can be significantly enhanced through association with mobile colloids (10-12). Radionuclides can adsorb strongly onto colloids through the same mechanisms by which they adsorb to stationary aquifer solids (13-15). Lieser et al. (16) reported Cs, Sr, Pb, Ac and Th adsorption onto and migration with inorganic colloids in groundwaters. Saiers and Hornberger (17) reported enhanced ¹³⁷Cs transport by kaolinite clay in soil columns. Kersting et al. (18) recovered colloid-associated plutonium in groundwater at a distance of 1.5 km away from a source area at the Nevada Test Site.

The objective of this research is to identify the major reactions and products resulted from leakage of REDOX TWS into underlying sediments, which are critical for assessing mechanisms controlling contaminant fate and transport at Hanford and other similar sites. Our general approach is to study subsurface tank-leakage as a coupled transport and geochemical process through simulating contamination events in laboratory sediment columns.

1. MATERIAL AND METHODS

2.1. Sediment Characterization

The sediment used for packing columns is “coarse sand”, a glaciofluvial sediment from the Hanford Formation, collected at the grout test site located in the eastern part of the 200 East Area of the Hanford site at a depth of about 1.5 to 3 m. This material is representative of sand facies of the Hanford Formation. The 200 East and 200 West Areas are the principal waste management areas and house high-level waste tanks. The Hanford Formation comprises about 85% of the vadose zone of the site. The sand facies are mostly coarse to medium sands, and contain scattered well-rounded pebbles and cobbles, with some thin discontinuous silt lenses (19). The minerals are derived from diverse sources of igneous, metamorphic, and sedimentary terraines. The major components are feldspar, quartz, and basaltic rock fragments (20–22). The sediment used in this study contains 87.4% sand, 10.3% silt, and 2.3% clay, with a density of 2.85 Mg m^{-3} . Calcium carbonate comprises 1.1% of the total mass. The clay-sized fraction is composed of 40% illite, 20% smectite, 20% mixed-layer illite and smectite, 20% kaolinite, with trace amounts of chlorite, as determined by X-ray diffraction. A water extract from the sediment (water to soil mass ratio = 1:1, at 21°C for 24 hours) was analyzed for major ions, and the results are shown in Table 1. A 10 fold dilution of the sediment extract was used as the formula of the leaching solution in the column experiments described in section 2.3 and 3.2.

Table 1. Composition of Water Extract of the Hanford Sediment (mM)

pH	EC	Na ⁺	K ⁺	Mg ²⁺	Ca ²⁺	Cl ⁻	SO ₄ ²⁻	HCO ₃ ⁻ , CO ₃ ²⁻
8.4	21.6 mS m ⁻¹	0.89	0.17	0.11	0.23	0.27	0.56	0.91

2.2. Simulated REDOX Tank Waste Solution (TWS)

The single-shell tanks contained waste solutions from the REDOX process of Pu and U recovery. During this process, aluminum nitrate solution was used to dissolve Pu and U from spent fuel. After extracting actinides, the residual acidic solution was treated with NaOH to keep aluminum in solution. The waste solution was then pumped into underground tanks for storage. A typical fresh REDOX waste solution was a 4 M sodium-nitrate-nitrite-aluminate-hydroxide solution (7). Upon self-boiling while in a waste tank, the original solution became more concentrated and formed salt cakes. Because different tanks leaked at different times and over different periods, accurate chemical compositions of TWS at the times of leaks are unknown. Agnew (4, 23) provided estimates of chemical compositions of the tank inventories based on a comprehensive review of tank histories. Our simulated TWS was formulated based on the composition of SX-111 (7). Three reasons motivated choosing this data set. Firstly, the SX-111 (Table 2) data are from direct measurements. It is one of a couple of available historical direct measurements of single shell tank waste solutions. Secondly, the chemical composition of SX-111 appeared to be a reasonable representation of leaked TWS, being within the middle range of Agnew's estimated composition of tank supernatant solutions. Thirdly, the solution was stable at room temperature over a long period of time. Our simulated TWS contained 0.8 M Al, 8 M Na, and 5 M NO_3^- , with pH of 14. All salts added were completely dissolved within hours of stirring at room temperature. The solution was filtered through a 0.45 μm filter before use. Radionuclides were not included in the simulated TWS because this study focused on effects of major chemical components.

Table 2. Major Chemical Components of SXT Waste Solutions

	The historical analyses of SX-111 (Molar)	Agnew's estimate (Molar)
Al	0.805	0.7 to 1.9
Cl	--	0.09 to 0.26
CO ₃	0.168	0.2 to 0.3
F	0.014	--
OH	1.47	3 to 8.5
NO ₃	4.72	2.3 to 6.3
NO ₂	0.84	1 to 2.9
PO ₄	0.0055	0.04 to 0.12
SO ₄	0.06	0.1 to 0.3
Na	8.05	5 to 14
Si	0.0015	--
density	1.37 Mg m ⁻³ *	--
viscosity	2.0 mPa s *	--
pH	14*	--

From Agnew (4, 23) and Serne et al. (7). * Our measurements.

2.3. Column Methodology

The acrylic plastic columns used to contain sediments were 3.8 cm inner diameter and 5 and 25 cm tall. Both end caps of a column had polypropylene screens (105 µm mesh opening) to support the sediment and allow the transport of suspended particles. Moistened sediments

(water content of 6% by mass) were packed homogeneously into columns to an equivalent dry bulk density of $1.65 (\pm 0.05) \text{ Mg m}^{-3}$, to represent the initial partially saturated vadose zone. To avoid gravity-induced flow fingering, solutions were injected upwards from the bottom of vertical columns, and the effluent samples were collected at the top. Therefore, the columns were practically saturated after the first pore volume of injection. The simulated TWS was injected by using a syringe pump at a pore-water velocity of 12 cm d^{-1} . In order to test possible colloid removal caused by rainfall, 9 pore volumes (PV) of the leaching solution (composition described in section 2.1, pH 7.4) was injected after 9 PV of TWS injection at the same flow rate. Since the sediment immediately underneath SXT experienced elevated temperatures, experiments were conducted at elevated and ambient temperatures. For the high-temperature tests, columns were set inside a sealed hot water bath, with the temperature controlled at $70 \pm 0.5^\circ\text{C}$. The lower temperature tests were conducted at room temperature ($21 \pm 1^\circ\text{C}$). Column effluents were collected into polypropylene tubes using a fraction collector, in 1/6 and 1/10 PV increments for the 5 and 25 cm long columns, respectively.

Solution pH, electrical conductivity (EC), and turbidity were measured within a day after the effluents were collected. For the 5 cm columns turbidity and pH were measured for additional two times, at 30 and 60 days after effluent collection. These later measurements were motivated by observed continued precipitation within the effluents. Measurements of pH were obtained using a non-glass pH probe (Sentron IntelliProbes). EC measurements were conducted on solutions that were 100-times diluted with distilled water. Samples were ultrasonicated to disperse aggregates of particles before obtaining turbidity measurements (Hach 2100 AN turbidity meter). Particle-size distributions and number concentrations were measured 60 days

after the effluents were collected using Multisizer II, (Coulter Co., Miami, FL) with a 50 μm orifice.

X-ray diffraction (Siemens D500) was used to identify structures and minerals in precipitates from different reaction stages (Powder Diffraction File, PDF-2, International Center for Diffraction Data, 1992). Precipitates were separated from effluent liquids with 0.25 μm filters, lightly rinsed with deionized water to remove excess soluble salts, and air-dried. The amount of precipitate recovered from the single fraction at the Reaction front stage was enough for XRD. In order to obtain enough mass (≥ 2 mg) of precipitates from the other reaction stages, precipitates were combined from multiple-fractions. Particle morphology was characterized using a scanning electron microscope (SEM Topcon DS130C). Energy dispersive x-ray microanalysis (EDS) was used for determining major elemental composition of individual particles (EDAX model DX-4). A transmission electron microscope (TEM) (Philips CM200/FEG) was used for micro-diffraction of some fine-sized particles that were not identifiable by XRD.

3. RESULTS AND DISCUSSION

In the following sections we present the pH, turbidity, and EC results from liquid effluent samples. Based on these data, three reaction stages of TWS and sediment interactions were identified. They are the reaction front stage (RFS), the early waste-plume stage (EPS), and the late waste-plume stage (LPS). The simulated rainfall event is presented as the leaching stage. Particle-size distributions and counts, mineralogy, and morphology of the precipitates collected from each reaction stage are also presented.

3.1. Tank waste solution breakthrough curves of pH, turbidity, and EC

Examples of typical breakthrough curves of TWS are presented in Figures 1 and 2, for the 5 and 25 cm columns, respectively. In each figure the left panel [panel (a)] shows breakthrough curves at 70°C, and the right panel [panel (b)] shows breakthrough curves at 21°C. In each panel, from top down, three breakthrough curves are shown: pH, turbidity, and normalized EC. Outflow did not appear until ~0.7 PV of TWS was infused, because of the low initial moisture content of the sediment (6 mass %). The normalized EC values refer to the electrical conductivity of 100-times diluted effluents, relative to that of the original TWS at the same dilution. The RFS is defined as the moving front of the waste-plume. The front of the waste-plume is identified using the inflection point of a measured EC curve, where high salinity TWS mixed with the initial soil solution. The first few effluent fractions (first two for the 5 cm and first four for the 25 cm columns) prior to the inflection point contained the original soil solution being displaced by TWS, as indicated by the EC and pH values. The pH of the first effluent fraction was about equal to that of the initial soil solution. Then, the pH decreased as the soil solution mixing with the waste plume front (RFS). A pH minimum appeared at the plume front, coincident with the inflection point of the EC curve. It was a surprise for us to see that the plume front had such a depressed pH, as low as 7.3. Clearly, simple mixing of the TWS (pH 14) with the soil solution (pH 8.4) could not result in such low pH. Acidity released by silicate dissolution is believed responsible for the steep pH reduction. Another outstanding characteristic at the RFS was the extremely high and narrow turbidity peak, indicating a large quantity of mobile particle formation and transport (see turbidity data in Figures 1 and 2). The highest turbidity occurred within the RFS at both temperatures and in all of the columns. Figure 3 shows

a typical, high turbidity, ambient temperature RFS effluent sample. Precipitate mass contents of 1.1 and 3.0 mass % were measured for two 21°C samples (precipitates retained on a 0.25 µm filter, lightly rinsed with deionized water, and air-dried). These two 21°C RFS samples had turbidities of 2,400 and 5,500 NTU, respectively. Peak turbidity values were always higher for lower temperature columns and for shorter columns. This is at least partly because particle transport was more limited at 70°C RFS due to the formation of larger sized aggregates than at the 21°C RFS (SEM images shown later). In addition, more filtration of suspended particles occurred in longer columns.

The pH val

TWS. The EPS is defined as the period of time when pH of effluents quickly recover to near the initial TWS pH. The EC curves showed trends similar to those of the pH curves. The LPS is defined as the period when the effluent pH returns to values very near that of the influent TWS. During this stage, the pH no longer changes significantly for the given flow rate, indicating only slow silicate dissolution. Increased turbidity values were measured over a period of 60 days after collection of effluents (Figure 1), with much larger increases from higher-temperature column effluents. This is consistent with effluents becoming supersaturated as their temperature fell from 70°C back to 21°C, followed by particle nucleation over time. For the 25 cm columns, turbidity changes over time were not measured.

3.2. Leaching solution breakthrough curves of turbidity and pH

In order to test possible removal of the secondary colloids during later rainfall, 9 PV of the leaching solution were injected after the TWS injection in the 5 cm columns. Figure 4 shows the leaching breakthrough curves (9 to 18 PV regions) of turbidity and pH at 70 (a) and 21°C (b). Data from the previous TWS effluents are also shown for comparison (0 to 9 PV). During the

leaching process pH declined gradually to about 11.7 after 9 PV. No significant particle transport was detected from the effluents analyzed immediately after collection ("day 0" data). Although particle release might be expected because of exposure to the much lower ionic strength leaching solution, dissolution of recently precipitated solids maintained the effluent ionic strength at levels high enough minimize colloid dispersion. Since the lowest pH value (11.7) achieved during leaching by itself contributes 5 mM to the ionic strength, "buffering" of ionic strength is evident even in the pH data. It is also worth noting that severe pore plugging and cementation within the columns were observed at the end of 9 PV of TWS injection, especially at 70°C. Even if some previously formed colloids were released by the leaching solution, their transport through such an altered medium would be less favorable. On the other hand, a small amount of new colloids formed within the leaching effluents long after their collection (see Figure 4, leaching stage data from day 30 and day 60 analyses). Nevertheless, net release and transport of secondary colloids during the leaching stage was relatively minor.

3.3. Particle-sizes and number concentrations

The data presented in Figure 5 are incomplete because the particle-sizer (Coulter Multisizer II) used with a 50 μm orifice has a lower size detection limit of 0.6 μm . The size and concentration measurements were conducted on particles recovered from the 5-cm columns at both temperatures, 60 days after effluent collection. Representative samples from the RFS, plume stage, and leaching stage were measured from each column. Since there were no significant morphology and mineralogy differences observed between the EPS and LPS precipitates (section 3.4), only one LPS effluent was measured. The peak turbidity fraction was used for the RFS. The fractions with highest turbidity within the LPS and the leaching stage

were selected for these measurements. Effluent samples were sonicated, subsampled, and diluted before particle-sizing.

The highest particle concentrations were always associated with the smallest quantifiable size-fraction, shown as peaks at 0.6 μm for all the samples measured (Figure 5). Greater than 90% of the RFS particles were in the colloid size range ($\leq 1.0 \mu\text{m}$). Particle sizes up to 10 μm for the waste plume stage, and up to 5 μm for the leaching stage were detected. Particle concentrations (numbers per volume) were 10-15 times higher in the RFS than during any other stages. Particle concentrations in the RFS were 6 times higher at 21°C than at 70 °C. However, higher particle concentrations eventually developed in the 70 °C effluents for the other stages because of greater precipitation from supersaturated solutions upon cooling. It is worth to note that the fine-sized RFS particles were primarily transported particles (based on turbidity data at day 0, as well as the observation during the effluent collection). The larger particles in the other stages were primarily precipitated after the effluents had been collected (turbidity data at day 30 and 60).

3.4 Morphology and Mineralogy of Precipitates

Representative XRD patterns, SEM images and x-ray microanalyses of chemical compositions for precipitates formed at different reaction stages are presented in Figures 6 to 10. Figure 6 provides information on RFS precipitates at 21°C. These precipitates were composed of two major phases: fine-grained particles and larger crystals (Figure 6a). During the experiments we observed the fine particles in the effluents during collection, while the large crystals formed after collection. The XRD analyses of the bulk samples could only characterize the larger calcite crystals (Figure 6b), but not the fine particles. Electron micro-diffraction by TEM was

conducted for the fine particles, but still revealed no diffraction pattern. Elemental analyses by SEM indicated that the amorphous phase was composed primarily of Al-Ca-Si-O with some Mg-Na-S (Figure 6c), and the crystal phase contained simply Ca-O (Figure 6d). Precipitates from the RFS at 70°C were vastly different from those at 21°C. The predominantly Si-O fine particles (tens of nanometers, Figure 7c) formed aggregates with shapes of hollow balls and flakes (Figure 7a,b). Results from both XRD and electron micro-diffraction by TEM indicate that these silica-dominant particles are amorphous. Calcite was also detected in the RFS at 70°C. However, aluminum was not detected in these precipitates.

Zeolites were the primary minerals formed in both the EPS and LPS under both temperatures, with a much larger quantities at 70°C (due to larger degree of silicate dissolution at higher temperature). At 21°C, zeolites were the only dominant phases identified, and no differences in mineralogy and morphology were identified between the EPS and LPS. However, at 70°C the color of effluent liquids and precipitates changed from light-brownish in the EPS to reddish in the LPS, and hematite was found. Figure 8a-d show the different morphology of precipitates formed in the plume stage. XRD identified the cubic crystals as zeolite, type A sodium form, $\text{Na}_2\text{Al}_2\text{Si}_{1.85}\text{O}_{7.7}\cdot 5.1\text{H}_2\text{O}$ (Figure 8e) (24). The spheres were identified as zeolite, cancrinite type, $\text{Na}_8(\text{Al}_6\text{Si}_6\text{O}_{24})(\text{NO}_3)_2\cdot 4\text{H}_2\text{O}$ (Figure 8f) (25). XRD did not detect structural differences among these different morphologies. In the high temperature LPS, an additional phase consisting of fine reddish particles (30-50 nm) were found sorbed on zeolites as shown in the SEM images (Figure 9a,b). Figures 9c and 9d present the major cation compositions of the zeolite and the sorbed reddish particles. No diffraction patterns were obtainable by XRD on these fine Fe-oxide particles. Electron micro-diffraction identified these particles as hematite. In the leaching stage, bayerite (Figure 10) was identified as the most abundant mineral.

Formation of bayerite only occurred when the solution pH reduced to below 12. Ettringite and calcite were also detected.

3.5 Implications for Radionuclide Transport

These laboratory simulations of REDOX tank waste solution leakage into underlying sediments revealed the main reaction stages, and their major products as secondary precipitates. The sediment undergoes three reaction stages: the RFS, the EPS, and the LPS. At the reaction front of the waste plume, maximum geochemical disequilibrium promoted rapid silicate dissolution, cation exchange of Na replacing Ca, and maximum precipitation. Rapid silicate dissolution upon exposure to the alkaline waste was responsible for the steep pH drop to levels below that of the initial soil solution. The neutralized alkalinity in turn induced massive precipitation of Al, which is only stable in the waste solution at high pH. The rapid precipitation of Al, Si, and Ca resulted in predominantly amorphous and submicron-sized secondary precipitates. Maximum transport of secondary colloids also occurred at the RFS, where colloids had the smallest sizes and some of them had not yet deposited onto primary grain surfaces, and where pores have not yet been plugged or cemented by the precipitates. Dissolution of primary minerals continued during the early waste plume stage, but at decreasing rates as indicated by the effluent pH rising back towards values close to that of the original waste solution. When the pH recovers to sufficiently high levels, Al again becomes stable in solution. Given enough time, zeolites and nitrate-cancrinite became the dominant precipitates throughout the entire waste plume stage. By the late plume stage, the coatings deposited from the earlier stage precipitation now are effective at protecting silicates from dissolution to such an extent that solution pH changes are no longer measurable.

The primary environmental concern over leakage from REDOX waste tanks remains associated with radionuclides rather than major ions. Because this is a complex reactive transport process, batch-based studies are insufficient for understanding and predicting relevant reactions. This study of major reaction stages provides the context within which REDOX radionuclide transport through the Hanford vadose zone can be better understood. The impact of these major reaction stages, especially the RFS, on radionuclide transport needs investigation, and this could be done through the addition of specific radionuclides (such as Cs) in similar laboratory tests. Radionuclides contained in the waste plume will exhibit varying degrees of co-precipitation or sorption on mobile colloidal phases in the RFS. Batch sorption tests only determine partitioning on radionuclides between solution and solid/surface phases, but yield no insights into potential mobility of the latter. Thus, effective retardation capacities of these secondary precipitates for radionuclides need to be directly measured under dynamic conditions representative of subsurface transport, i.e., through column experiments similar to those presented here.

The amorphous RFS precipitates and the plume stage zeolites and cancrinite are most likely to retard radionuclide transport by sorption and co-precipitation. Recall that significant pore plugging and cementation by the secondary precipitates were observed, and was more extensive at higher temperature and with exposure to larger fluxes of waste solution. The post-plume leaching with dilute soil solutions did not remove significant amounts of previously generated-deposited colloids. Even if particles are locally released, alteration of the sediment from reactions favors colloid recapture. A coupled geochemical and transport model with the capability of correctly representing high salinity solutions and suspensions is necessary to simulate these experimental findings, and to predict these processes and their effects on contaminant transport at larger scales.

Acknowledgments

This work was carried out under U.S. Department of Energy Contract No. DE-AC03-76SF-00098. Funding is provided by the Environmental Management Science Program. The authors thank Jeff Serne and George Last (PNNL), Tom Jones (the Hanford Site) and Peter Persoff (LBNL) for providing the Hanford vadose zone sediments and information about the sediments and tank waste liquids. We also thank Eric Sonnenthal for the helpful internal review of this manuscript.

References

- (1) Riley, R. G.; Zachara, J. M.; Wobber, F. J. Chemical contaminants on DOE lands and selection of contaminant mixtures for subsurface science research, DOE Office of Energy Research Subsurface Science Program, **1992**, DOE/ER-0547T.
- (2) DOE. Vadose zone characterization project at the Hanford Tank Farms-SXTank Farm. DOE/ID/12584-268, U. S. Department of Energy, **1996**, Grand Junction, Colorado.
- (3) Ward, A. L.; Gee, G. W.; White, M. D. A comprehensive analysis of contaminant transport in the vadose zone beneath tank SX-109, PNNL-11463, **1997**, Pacific Northwest National Laboratory, Richland, Washington.
- (4) Agnew, S. F. LA-UR-94-2657, Rev. 2, **1995**, Los Alamos National Laboratory, Los Alamos, NM.
- (5) Jones, T. E.; Maclean, G.T. Inventory estimates for single-shell tank leaks in S and SX tank farms, RPP-6285, Rev. 0. **2000**, CH2MHILL Hanford Group, Inc., Richland, Washington.
- (6) Lichtner, P. C. and A. Felmy, Estimation of Hanford SX Tank Waste Compositions from Historically Derived Inventories, Computers & Geosciences, **2002**, in press.
- (7) Serne, R. J.; Zachara, J. M.; Burke, D. S. Chemical information on tank supernatants, Cs adsorption from tank liquids onto Hanford sediments, and field observations of Cs migration from past tank leaks, PNNL-11495, **1998**, Pacific Northwest National Laboratory, Richland, Washington.
- (8) Nyman, M.; Krumhansl, J. L.; Zhang, P.; Anderson, H.; Nenoff, T. M. Mater. Res. Soc. Symp. Proc. **2000**. 608, 225-230.

- (9) Bickmore, B. R.; Nagy, K. L.; Young, J. S.; Drexler, J. W. *Environ. Sci. Technol.* **2001**, *35*, 4481-4486.
- (10) Buddemeier, R. W.; Hunt, J. R. *Appl. Geochem.*, **1988**, *3*, 535-548.
- (11) McCarthy, J. F.; Zachara, J. M. *Environ. Sci. Technol.* **1989**, *23*, 496-502.
- (12) Harvey, R. W.; George, L. H.; Smith, R. L.; LeBlanc, D. R. *Environ. Sci. Technol.* **1989**, *23*, 51-56.
- (13) Sheppard, J. C.; Campbell, M. J.; Cheng, T.; Kittrick, J. A. *Environ. Sci. Technol.* **1980**, *14*, 1349-1353.
- (14) Shade, J. W.; Ames, L. L.; McGarrah, J. E. in *Geochemical Behavior of Disposed Radioactive Waste*, Barney, G. S.; Navratil, J. D.; Schulz, W. W. (eds.), Amer. Chem. Soc. Symp. **1984**, Ser. 246, 67-77. American Chemical Society, Washington, DC.
- (15) Nelson, D. M.; Penrose, W. R.; Karttunen, J. O.; Mehlhaff, P. *Environ. Sci. Technol.*, **1985**, *19*, 127-131.
- (16) Lieser, K. H.; Ament, A.; Hill, R.; Singh, R.N.; Stingl, U.; Thybusch, B. *Radiochimica Acta*, **1990**, *49*, 83-100.
- (17) Saiers, J. E.; Hornberger, G. M. *Water Resour. Res.*, **1996**, *32*, 33-41.
- (18) Kersting, A. B.; Efurud, D. W. Finnegan, D. L.; Rokop, D. J.; Smith, D. K.; Thompson, J. L. *Nature*, **1999**, *397*, 56-59.
- (19) Swanson, L.C.; Weeks, D. C.; Luttrell, S. P.; Mitchell, R. M.; Landeen, D. S.; Johnson, A. R.; Roos, R. C. Grout Treatment Facility Environmental Baseline and Site Characterization Report, WHC-EP-0150, **1988**, Westinghouse Hanford Company, Richland, Washington.
- (20) Serne, R. J.; Zachara, J. M.; Burke, D. S. Chemical information on tank supernatants, Cs adsorption from tank liquids onto Hanford sediments, and field observations of Cs migration

from past tank leaks, PNNL-11495, **1998**, Pacific Northwest National Laboratory, Richland, Washington.

- (21) Reidel, S. P.; Horton, D. G. Geologic Data Package for 2001 Immobilized Low-Activity Waste Performance Assessment, PNNL-12257, Rev. 1, **1999**, Pacific Northwest National Laboratory, Richland, Washington.
- (22) Serne, R. J.; LeGore, V. L.; Last, G. V.; Schaef, H. T.; O'Hara, M. J.; Smith, S. C.; Bjornstad, B. N.; Brown, C. F.; Lindenmeier, C. W.; Williams, B. A.; Parker, K. E.; Zachara, J. M.; Lanigan, D. C.; Kutnyakov, I. V.; Burke, D. B.; Horton, D. G.; Serne, J. N.; Clayton, R. E.; Mitroshkov, A. V. Characterization of Uncontaminated Sediments from the Hanford Reservation-RCRA Borehole Core Samples and Composite Samples, Prepared for the U.S. Department of Energy, **2001**, under Contract DE-AC06-76RLO 1830.
- (23) Agnew, S. F.; Boyer, J.; Corbin, R. A.; Duran, T. B.; Fitzpatrick, J. R.; Jurgensen, K. A.; Ortiz, T. P.; Young, B. L. Hanford tank chemical and radionuclide inventories: HDW Model Rev. 3. LA-UR-96-858, **1996**, Los Alamos National Laboratory, Los Alamos, NM.
- (24) Milton, R. US Patent, **1959**, 2, 882, 243.
- (25) Hund, F. Z. *Anorg. Allg. Chem.*, **1984**, 509, 153.

Figure Captions

Figure 1. Tank waste solution breakthrough curves of pH, turbidity, and EC for 5-cm columns at (a) 70°C, (b) 21°C.

Figure 2. Tank waste solution breakthrough curves of pH, turbidity, and EC for 25-cm columns at (a) 70°C, (b) 21°C.

Figure 3. A typical 21°C reaction-front stage effluent containing 3% (dry mass) particles (Tube 2). Tube 1 contains the original tank waste solution (clear solution).

Figure 4. Tank waste solution injection followed by a leaching solution. The breakthrough curves of pH and turbidity for 5-cm columns at (a) 70°C, (b) 21°C.

Figure 5. Particle-size distributions and counts of effluents collected from 5-cm columns at 21°C and 70°C at different reaction stages. Particles smaller than 0.6 μm were not detectable with the instrument used.

Figure 6. Precipitates formed at 21°C reaction-front stage. (a) SEM microphotograph showing two major phases: amorphous and crystal phases. (b) XRD pattern of the bulk precipitates. (c) Chemical composition of the amorphous phase. (d) Chemical composition of the crystal phase.

Figure 7. Precipitates formed at 70°C reaction-front stage. SEM microphotographs showing aggregates in shapes of (a) hollow balls and (b) flakes of amorphous fine particles. (c) The amorphous phase composed of predominantly Si-O.

Figure 8. Precipitates of waste plume stage. (a-d) SEM microphotographs showing different morphology. (e, f) XRD patterns.

Figure 9. Precipitates formed at 70°C late plume stage. (a) SEM microphotograph showing fine particles sorbed on zeolites. (b) A close view of these fine particles. (c) Chemical composition of zeolite. (d) Chemical composition of sorbed Fe-rich particles.

Figure 10. Precipitates formed during the leaching stage. (a) SEM microphotograph showing bayerite as the major phase. (b) XRD pattern of the bulk precipitates.

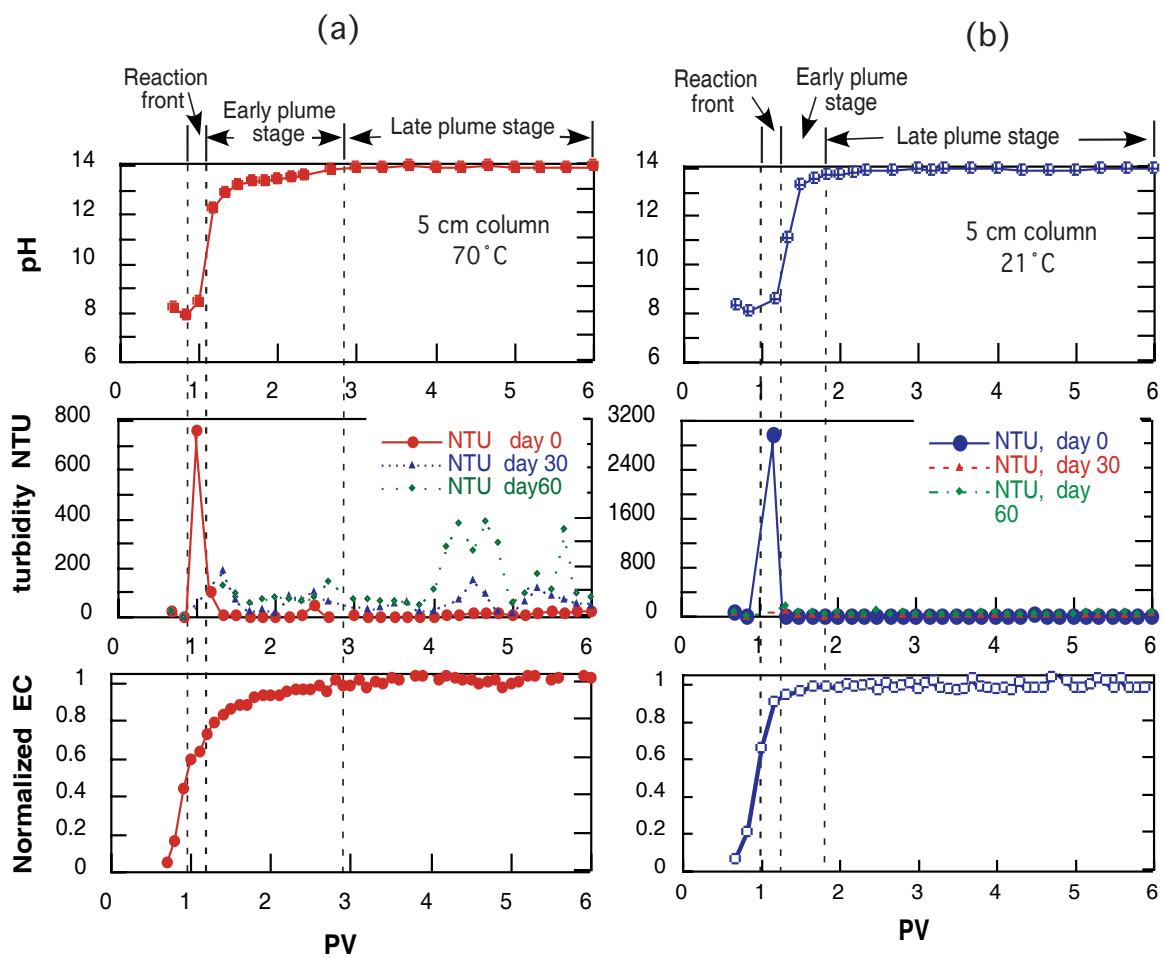


Figure 1.

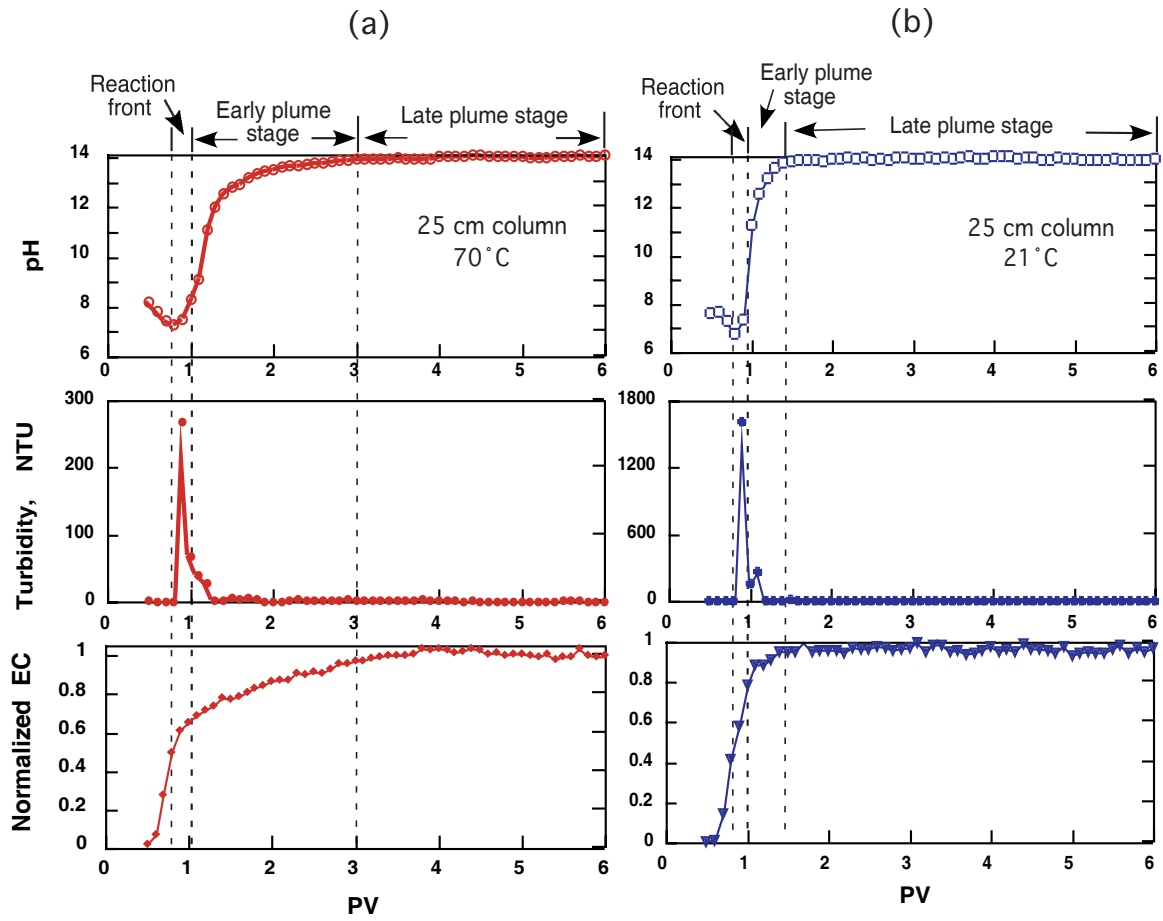


Figure 2.

Figure 3.

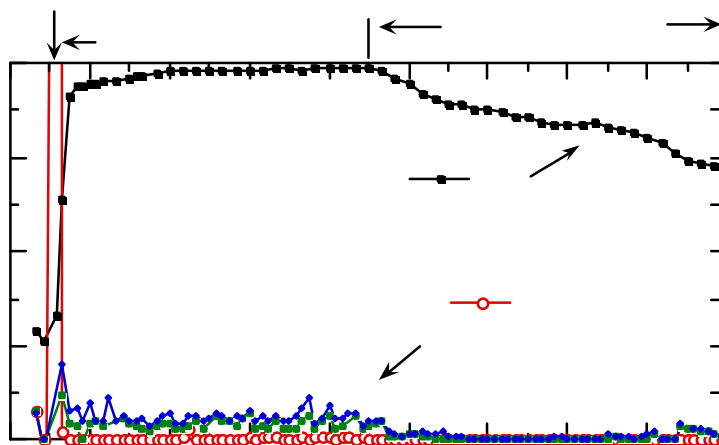
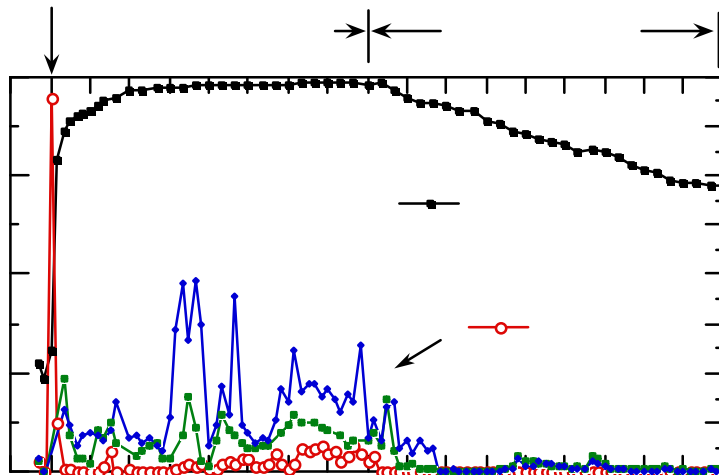


Figure 4.

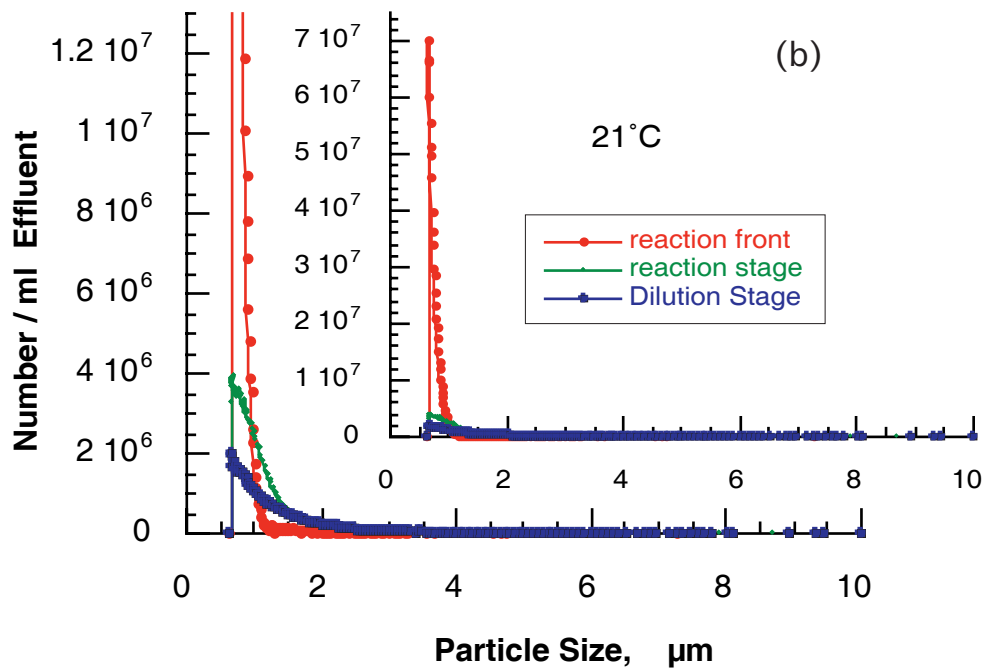
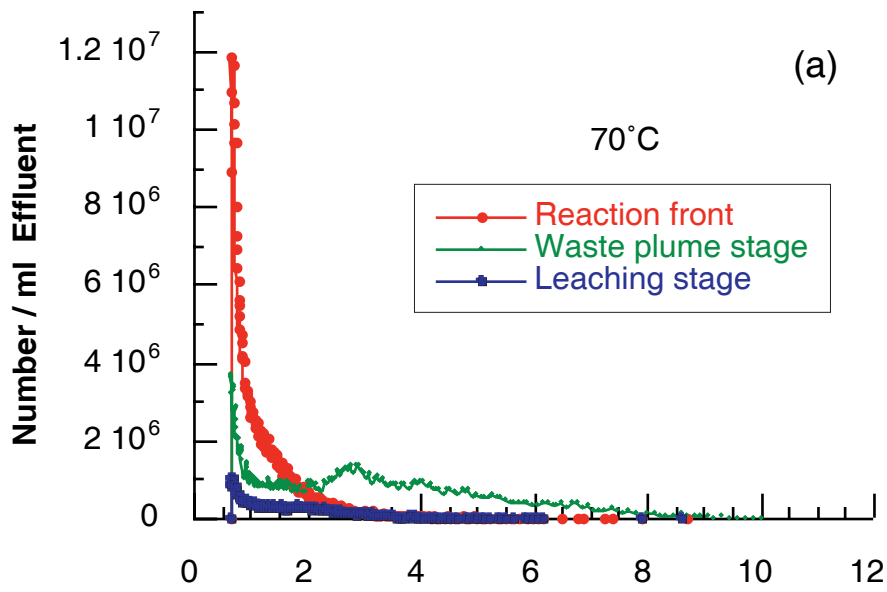


Figure 5.

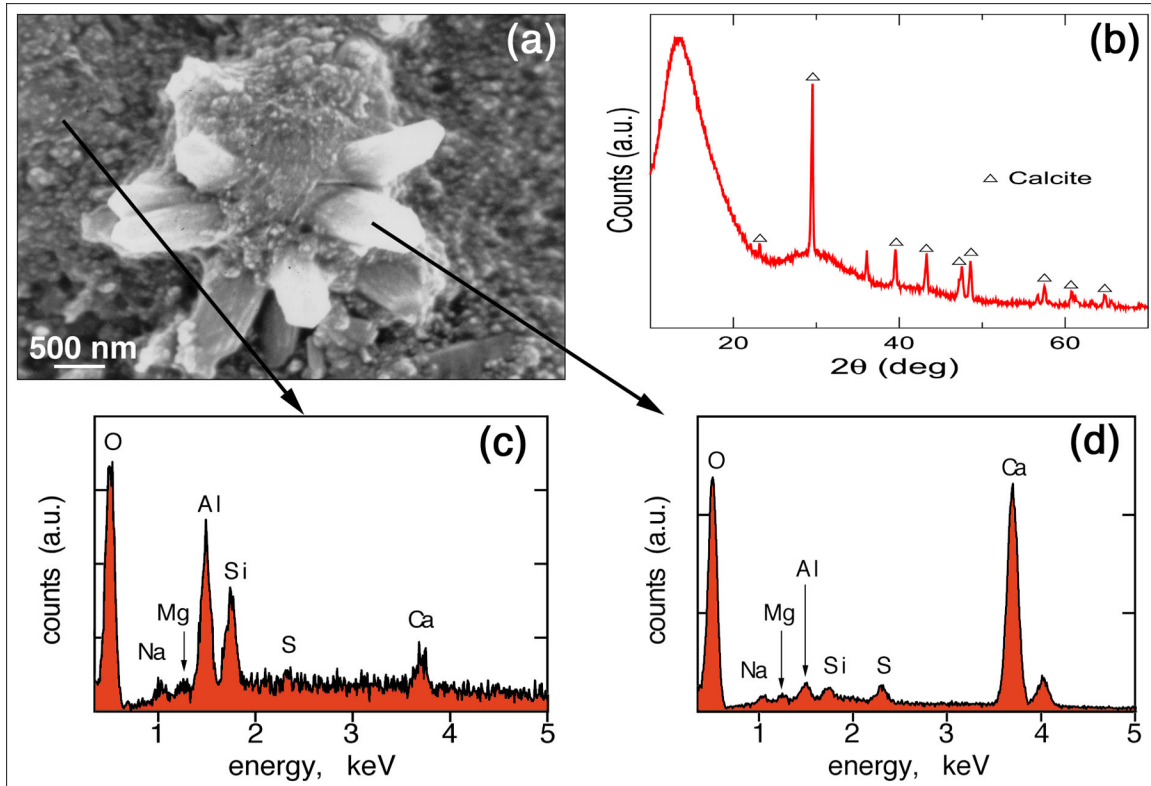


Figure 6.

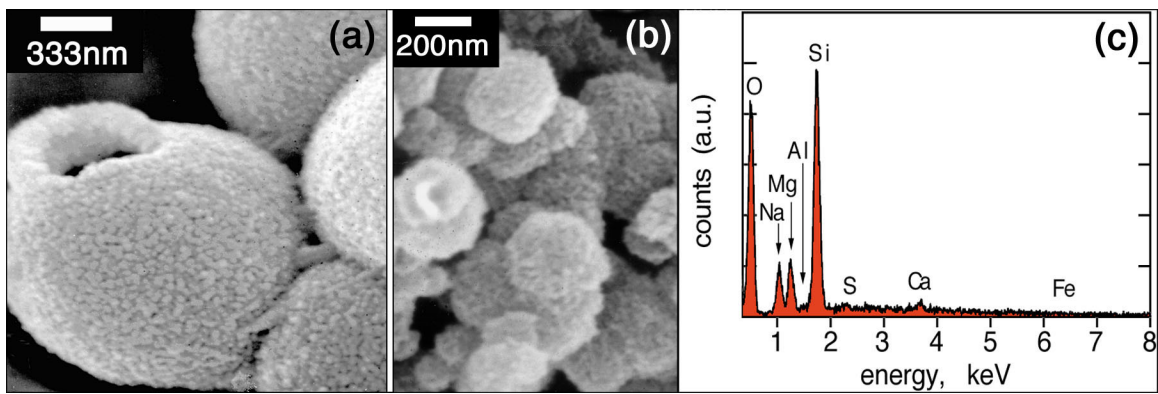


Figure 7.

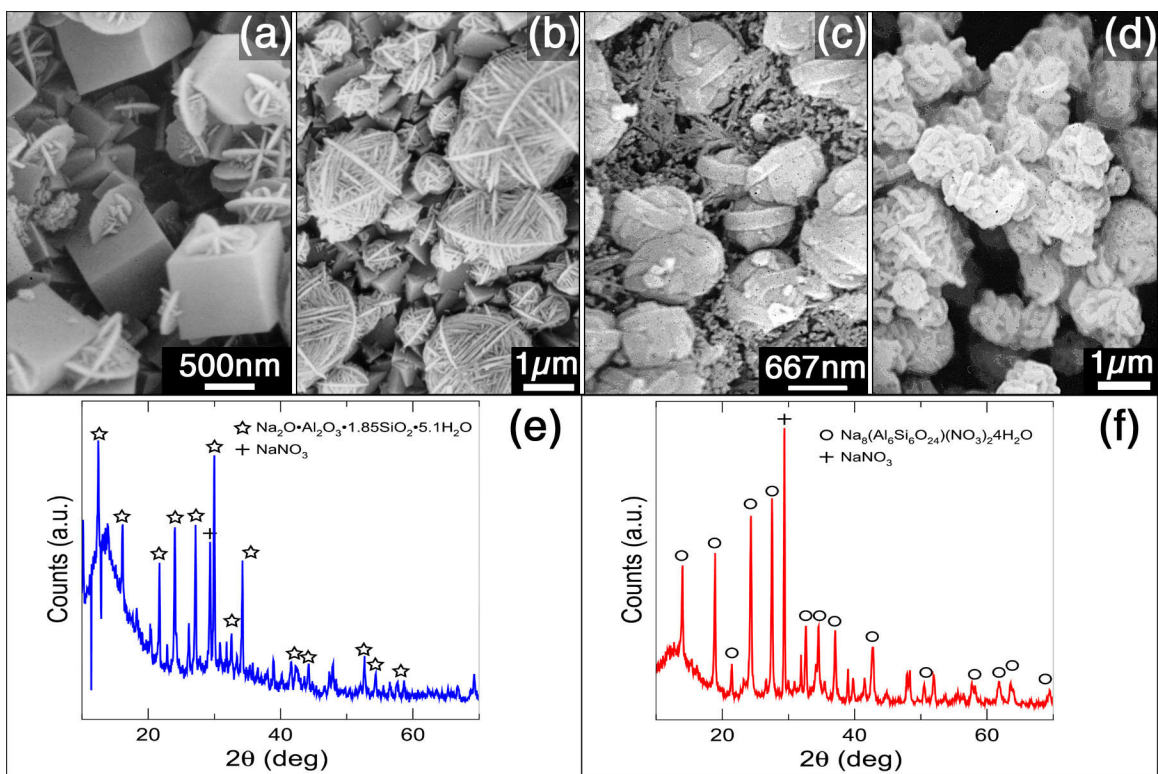


Figure 8.

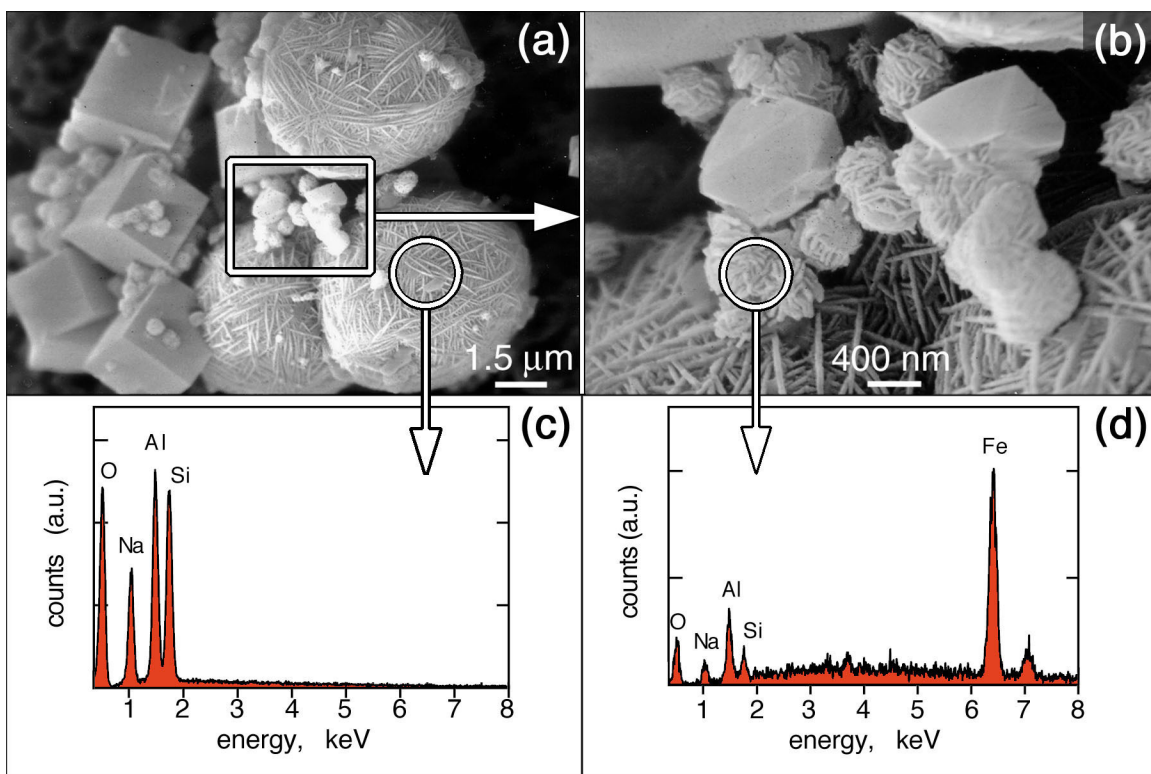


Figure 9.

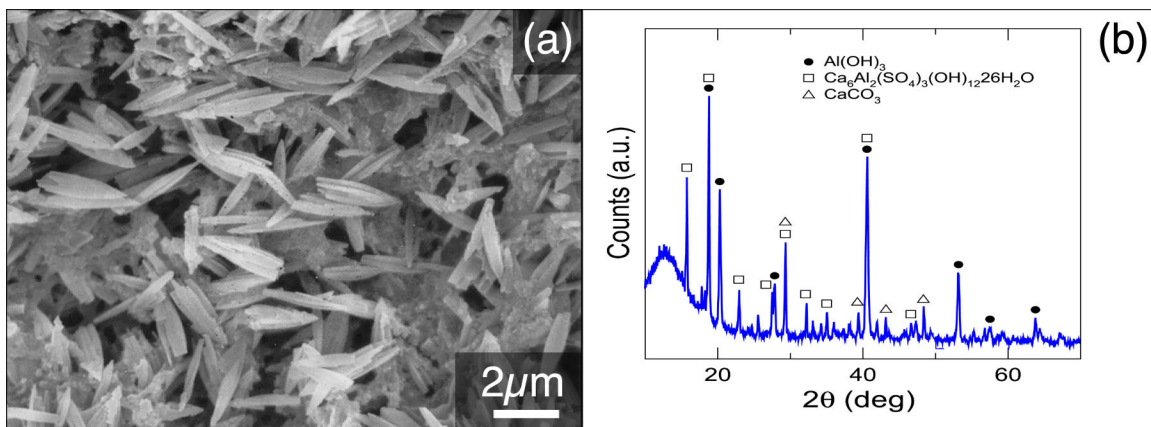


Figure 10.